Electronic Supporting Information for the paper

Elucidation of ^{1}H-NMR paramagnetic features of heterotrimetallic lanthanide(III)/manganese(III) 12-MC-4 complexes

Corrado Atzeri,[a] Vittoria Marzaroli,[a] Martina Quaretti,[a] Jordan R. Travis,[b] Lorenzo Di Bari,*[c] Curtis M. Zaleski,*[b] and Matteo Tegoni*[a]

Calculation of Lanthanide Induced Shift from ^{1}H NMR data

The observed chemical shift (δ^{obs}) for each proton (*i.e.* of each signal in the spectrum) is the sum of paramagnetic (δ^{para}) and diamagnetic (δ^{dia}) contributions as

$$\delta^{obs} = \delta^{para} + \delta^{dia} \quad (1)$$

In the hypothesis that the spin systems of the $[Mn^{III}]_4$ and that of the lanthanides are independent (*e.g.* small or negligible coupling)

$$\delta^{para} = \delta^{para}_{Ln} + \delta^{para}_{Mn} \quad (2)$$

where δ^{para}_{Ln} and δ^{para}_{Mn} are the paramagnetic shift contributions of the Ln^{III} and $[Mn^{III}]_4$ spin systems on each proton, respectively. The term δ^{para}_{Ln} is the Lanthanide Induced Shift (LIS). Since both terms eq. 2 contain a pseudocontact and a Fermi contact contribution, we may split the right member of eq. 2 into:

$$\delta^{para} = \delta^{con}_{Ln} + \delta^{PC}_{Ln} + \delta^{con}_{Mn} + \delta^{PC}_{Mn} \quad (3)$$

Therefore for a specific Ln^{III}-MC, it results (from eqs. 1 and 4):

$$\delta^{obs}_{Ln} = \delta^{con}_{Ln} + \delta^{PC}_{Ln} + \delta^{con}_{Mn} + \delta^{PC}_{Mn} + \delta^{dia} \quad (4)$$

In the case of Y^{III}–MC ion where the encapsulated ion is diamagnetic, the first two terms are zero and therefore eq. 4 reduces to:

$$\delta^{obs}_{Y} = \delta^{con}_{Mn} + \delta^{PC}_{Mn} + \delta^{dia} \quad (5)$$

Since the compounds are isostructural, we may also put forward the hypothesis that, for different Ln^{III} ions, the right terms in eq. 4 do not vary appreciably along the series of compounds. Under these circumstances, by combining eq. 4 and 5, we obtain:

$$\delta^{obs}_{Ln} = \delta^{con}_{Ln} + \delta^{PC}_{Ln} + \delta^{obs}_{Y} = \delta^{para}_{Ln} + \delta^{obs}_{Y} \quad (6)$$

which can be rearranged into

$$\delta^{obs}_{Ln} - \delta^{obs}_{Y} = \delta^{con}_{Ln} + \delta^{PC}_{Ln} = \delta^{para}_{Ln} = LIS \quad (7)$$

Therefore, the Lanthanide Induced Shift on the signal if each *i* proton can be calculated by subtracting the chemical shift observed for the Y^{III}–MC from that observed for a considered Ln^{III}-MC. This calculation has to be performed for all signals, and therefore eq. 7 will be used in the form

$$\delta^{obs}_{Ln}(i) - \delta^{obs}_{Y}(i) = \delta^{con}_{Ln}(i) + \delta^{PC}_{Ln}(i) = \delta^{para}_{Ln}(i) = LIS(i) \quad (8)$$

where *i* indicates the considered proton signal (*i*=1,2,3,4 for shi^{3-}, Me for acetates, see Figure 3). The calculated $\delta^{para}_{Ln}(i)$ values are reported in Table 1.

Development of a model for the enhancement in the electronic relaxation rate in Gd^{III}-MC

When two paramagnetic ions are present in the same system, in the absence of magnetic coupling one will have a longer relaxation time and the other will have a shorter one. Here M1 indicates the slow relaxing metal ion (Gd^{III}), while M2 indicates the fast relaxing one (Mn^{III}).

We have first evaluated if the coupling between the S1 and S2 spin systems has a contribution which is dipolar in origin, by calculating the electronic relaxation rate of the slow relaxing metal ion ($\Delta\tau_{s1,dip}^{-1}$) using the equation:[1]

$$\Delta\tau_{s1,dip}^{-1} = \frac{2}{15}\left(\frac{\mu_0}{4\pi}\right)^2\left(\frac{1}{\hbar}\right)^2\frac{g_e^4\mu_B^4 S_2(S_2+1)}{\langle r^3\rangle^2}\times\left[\frac{\tau_{s2}}{1+(\omega_{S1}-\omega_{S2})^2\tau_{s2}^2}+\frac{3\tau_{s2}}{1+\omega_{S1}^2\tau_{s2}^2}+\frac{6\tau_{s2}}{1+(\omega_{S1}+\omega_{S2})^2\tau_{s2}^2}\right]$$

In this equation, μ_0 is the permeability of vacuum, g_e the free-electron *g* factor, μ_B the Bohr magneton and $\langle r^3\rangle$ the average cube of the interelectronic distance, approximated with the Gd-Mn distance (ca. 3.8 Å). Also, S_2 is the total spin state of the fast relaxing metal ion, τ_{s2} its electronic relaxation time constant, and ω the Larmor frequencies of the two metals.
the case of M_1 = Gd^{III} and M_2 = Mn^{III} at 9.4 T (400 MHz), ω_{S1} and ω_{S2} are -1.01x10^{-6}‡ and 6.25x10^{-6} rad s^{-1}, respectively. In the absence of detailed information on the parameters related to the coupling between the Mn^{III}-Mn^{III} and Gd^{III}-Mn^{III} centers (i.e. $J_{Gd\text{-}Mn}$ and $J_{Mn\text{-}Mn}$ values), we have considered a simplified model where Gd^{III} interacts with only one Mn^{III}, the latter with S_2 = 2. Moreover, since we have observed a line broadening effect in the low boundary for this ion, we made the hypothesis that τ_{s2} is *ca*. 10^{-11} s.[2–6] Under these approximations, it resulted $\Delta\tau_{s1,dip}^{-1}$=2.8x10^9 s^{-1}, which is not negligible for Gd^{III}. In the further hypothesis that for uncoupled Gd^{III} τ_{s1}^{-1}= 10^8 s^{-1}, the value of $\tau_{s1,dip}^{-1}$ results 5.2 x 10^9 s^{-1}.

We have next evaluated the enhancement in the electronic relaxation rate of Gd^{III} arising from a scalar coupling ($\Delta\tau_{s1,con}^{-1}$). Since Gd^{III} and Mn^{III} are bridged by a single oxygen atom, we believed this interaction could be not negligible. We have evaluated this type of interaction using equation:[1]

$$\Delta\tau_{s1,con}^{-1} = \frac{2}{3}S_2(S_2+1)\left(\frac{J_{Gd-Mn}}{\hbar}\right)^2\frac{\tau_{s2}}{1+(\omega_{S1}-\omega_{S2})^2\tau_{s2}^2}$$

This equation contains the information on the $|J_{Gd\text{-}Mn}|$, which is unknown. We have initially considered a $|J_{Gd\text{-}Mn}|$ = 0.045 cm^{-1} since using this value it resulted $\Delta\tau_{s1,con}^{-1}$ = 2.9x10^9 s^{-1}, and therefore $\tau_{s1,con}^{-1} \approx \tau_{s1,dip}^{-1}$. However, this parameter was later varied in order to simulated the observed NMR linewidths.

The next step was to consider the total Gd^{III} electronic relaxation time as $\tau_{s1}^{-1} = \tau_{s1,dip}^{-1} + \tau_{s1,con}^{-1}$ = 5.9 x 10^9 s^{-1} (corresponding to τ_{s1} = 1.7x10^{-10} s). In the initial assumption that the correlation time τ_c is dominated by the contribution of electronic relaxation ($\tau_c \approx \tau_{s1} = 1/\tau_{s1}^{-1}$), we have evaluated the expected linewidth of the different protons of shi^{3-}. We limited this analysis to the dipolar electron-nucleus coupling, since the evaluation of the contact contribution requires the knowledge of the contact coupling constant which is unknown, although it is expected to be small for the aromatic protons. For the same reason we excluded the analysis of the linewidths of the CH_3 protons of acetates since for them the contact relaxation contribution might be dominant.

To evaluate the transverse relaxation rates of the protons (^1H = *I*, electron = *S*) we used the equation:

$$R_{2M} = \frac{1}{15}\left(\frac{\mu_0}{4\pi}\right)^2\left(\frac{1}{\hbar}\right)^2 \frac{\gamma_I^2 g_e^2 \mu_B^2 J(J+1)}{r^6} \times \left[4\tau_c + \frac{\tau_c}{1+(\omega_I-\omega_S)^2\tau_c^2} + \frac{3\tau_c}{1+\omega_I^2\tau_c^2} + \frac{6\tau_c}{1+(\omega_I+\omega_S)^2\tau_c^2} + \frac{6\tau_c}{1+\omega_S^2\tau_c^2}\right]$$

Where *J* = 7/2 for Gd^{III}, and r the Gd-H distance (obtained from the crystal structure).

Finally, the linewidth of a proton signal in the spectrum of Gd^{III}-MC ($\Delta\nu_{Gd-MC}$) was calculated as:

$$\Delta\nu_{Gd-MC} = \frac{R_{2M}}{\pi}$$

Using an initial value of $\tau_{s1}^{-1} = \tau_c^{-1}$ = 6.6 x 10^9 s^{-1} (obtained using a hypothetical $|J_{Gd\text{-}Mn}|$ = 0.045 cm^{-1}, see above) the calculated linewidths for the shi^{3-} protons were in the 300-1600 Hz range, quite close to those observed experimentally (see Table S1).

However, since the linewidths observed for of Y^{III}-MC (there the only paramagnetic system present is $[Mn^{III}]_4$) and Gd^{III}-MC are quite similar for the shi^{3-} protons (Table S1), we believe that the linewidths can be better evaluated using the equation:

$$\Delta\nu_{Gd-MC} = \frac{R_{2M}}{\pi} + \Delta\nu_{Y-MC}$$

Where $\Delta\nu_{Y-MC}$ are the linewidths in the spectrum of Y^{III}-MC. By varying the value of $|J_{Gd\text{-}Mn}|$ we found that the calculated linewidths closest to those observed experimentally (Table S1) were obtained for $|J_{Gd\text{-}Mn}|$ *ca*. 0.047 cm^{-1} (774, 484, 175 and 158 Hz for signals 1 to 4, respectively).

Procedure for calculation of the crystal field splitting parameter B_0^2

The calculation of the crystal field splitting parameter B_0^2 has been carried out using the equation reported in the literature:[7,8]

$$\delta_{Ln}^{PC}(i) = \frac{C_j \mu_B^2}{60(kT)^2} B_0^2 \frac{3cos^2\theta_i - 1}{r_i^3} 10^6 = \frac{C_j \mu_B^2}{60(kT)^2} B_0^2 \cdot G(i) \cdot 10^6 \quad (9)$$

By rearranging this equation, and taking into account that G(i) = $\frac{3cos^2\theta_i - 1}{r_i^3}$, we obtain

$$B_0^2 = \delta_{Ln}^{PC}(i) \cdot \frac{60(kT)^2}{C_j \mu_B^2} \frac{1}{G(i)} 10^{-6} \quad (11)$$

For a specific Ln^{III}-MC the calculated B_0^2 parameter should precisely result into the same value irrespective of the proton under examination (A-D, Figure 3). Since this does not occur because of the experimental nature of NMR data, we calculated the B_0^2 parameter for each Ln^{III}-MC taking into account the chemical shift of all shi^{3-} protons in the same treatment. This was carried out by least-square regression, by minimizing the function

$$\sum_{i=1}^{4} \left\{ \left(\delta_{Ln}^{PC}(i)\right)^{obs} - \left(\delta_{Ln}^{PC}(i)\right)^{calc} \right\}$$

where $\left(\delta_{Ln}^{PC}(i)\right)^{obs}$ are the values reported in Table 2, while $\left(\delta_{Ln}^{PC}(i)\right)^{calc}$ are the values calculated through eq. 9, using B_0^2 as the only fitting parameter. The G(i) terms we used are the <G(i)> values reported in Table S3. We also took into account the assignment of the signals in the spectra, which correspond (proton, signal) to (A, 2), (B, 4), (C, 3), (D, 1). See text, Figure 7 for further details. The calculated B_0^2 values for the Ln^{III}-MC (Ln^{III} = Tb^{III}-Yb^{III}) are reported in Table 4.

Table S1: T_1 spin-lattice relaxation constants and signal bandwidths for the proton signals in the spectra of the $Ln^{III}Na^{I}(OAc)_4[12\text{-}MC_{Mn^{III}(N)shi}\text{-}4](H_2O)_4 \cdot 6DMF$ in deuterated methanol (see Figure 3 for numbering and labelling).[a]

		Signal				
Ln^{III}		**Me**	**1**	**2**	**3**	**4**
Y^{III}-MC	δ , ppm	27.8	10.4	-16.9	-20.5	-24.3
	T_1, ms	2.35(1)	1.30(2)	1.48(1)	6.54(1)	7.36(1)
	ν½, Hz	360	290	250	60	70
Pr^{III}-MC	δ , ppm	29.1	9.7	-15.1	-19.1	-23.1
	T_1, ms	2.22(2)	1.33(1)	1.55(1)	7.08(4)	7.79(4)
	ν½, Hz	987	270	244	61	67
Nd^{III}-MC	δ , ppm	28.9	10.1	-15.6	-19.6	-23.5
	T_1, ms	1.90(4)	1.01(2)	1.25(1)	5.70(5)	6.30(1)
	ν½, Hz	1270	380	330	100	80
Sm^{III}-MC	δ , ppm	27.8	10.6	-16.5	-20.2	-24.0
	T_1, ms	3.3(5)	1.5(2)	1.53(1)	6.83(2)	7.50(2)
	ν½, Hz	650	290	240	60	90
Eu^{III}-MC	δ , ppm	27.9	10.5	-16.7	-20.5	-24.3
	T_1, ms	2.32(2)	1.50(2)	1.43(1)	6.81(2)	7.55(2)
	ν½, Hz	680	380	310	100	120
Gd^{III}-MC	δ , ppm	27.8	10.1	-16.5	-20.5	-24.2
	T_1, ms	0.14(1)	0.66(2)	0.93(4)	3.06(5)	3.35(5)
	ν½, Hz	2090	790	450	170	170
Tb^{III}-MC	δ , ppm	17.6	26.2	-5.5	-12.7	-17.4
	T_1, ms	1.10(2)	1.19(1)	1.34(1)	6.08(6)	6.80(7)
	ν½, Hz	910	430	390	140	130
Dy-MC	δ , ppm	20.2	22.9	-7.8	-14.4	-18.9
	T_1, ms	0.70(2)[b]	0.93(5)[b]	1.8(4)	5.1(3)	5.5(3)
	ν½, Hz	890	490	370	170	150
Ho^{III}-MC	δ , ppm	22.7	17.8	-11.3	-16.9	-21.1
	T_1, ms	1.04(1)	1.10(1)	1.38(1)	6.03(3)	6.74(4)
	ν½, Hz	880	340	310	100	100
Er^{III}-MC	δ , ppm	33.1	n.d.[c]	-21.2	-23.8	-27.1
	T_1, ms	1.17(1)	n.d.[c]	1.42(1)	6.23(1)	7.02(1)
	ν½, Hz	780	n.d.[c]	310	90	90
Tm^{III}-MC	δ , ppm	47.8	-5.3	-27.4	-27.9	-30.7
	T_1, ms	2.1(4)	1.3(2)	n.d.[d]	n.d.[d]	7.0(1)
	ν½, Hz	760	450	440	220	150
Yb^{III}-MC	δ , ppm	31.0	6.3	-19.7	-22.6	-26.1
	T_1, ms	2.15(1)	1.34(1)	1.53(1)	7.13(1)	7.83(1)
	ν½, Hz	540	390	260	70	70

[a] In the case of partially overlapped peaks (*i.e.* in the spectra of Dy^{III}-MC and Tm^{III}-MC) the bandwidth at half-height ($\nu_{½}$, Hz) was determined by treatment of the fitting curves (blue lines, Figures S1 and S2).

[b] The determination of T_1 for the partially overlapped signals of the Dy^{III}-MC was obtained by treating the integral of the tails of the signals with the function of the Inversion Recovery.

[c] Signal not visible as covered by solvent peaks.

[d] T_1 value was not calculated due to the significant coalescence of the peaks.

Table S2. Average distances ($r_{Ln..H}$) and angles with respect of the molecular axis ($\theta_{Na\text{-}Ln\text{-}H}$) for the shi^{3-} protons in the Gd^{III}/Yb^{III}-MC series (see labelling in Figure 3 and here below). Data obtained from the X ray crystal structure (see ref. [9]). The angles between the nucleus under consideration and the principal magnetic axis of the lanthanide ion has been approximated into the Na^{I}-Ln^{III} direction. Distances and angles have been averaged for each proton in the four shi^{3-} ligands.

	$r_{Ln..H}$ (Å)				$\theta_{Na\text{-}Ln\text{-}H}$ (°)			
	A	**B**	**C**	**D**	**A**	**B**	**C**	**D**
Gd	7.936	9.310	8.930	6.981	114.55	113.05	111.77	112.78
Tb	7.811	9.296	8.916	6.965	114.47	111.99	111.72	112.68
Dy	7.919	9.294	8.914	6.962	114.32	112.85	111.59	112.53
Ho	7.909	9.284	8.903	6.951	114.20	112.75	111.52	112.41
Er	7.901	9.275	8.894	6.945	114.21	112.77	111.49	112.38
Tm	7.892	9.264	8.882	6.938	114.13	112.71	111.48	112.34
Yb	7.896	9.272	8.888	6.938	114.11	112.72	111.44	112.28

Table S3. Average <G(i)> terms for the shi^{3-} protons in the Gd^{III}/Yb^{III}-MC series, calculated using the X ray structural data (see labelling in Figure 3 and here below).[9] The G(i) values have been averaged using the individual values for the protons in the four shi^{3-} ligands.

	<G(i)> (10^{20} cm^{-3})			
	A	**B**	**C**	**D**
Gd	-9.64	-6.66	-8.16	-16.1
Tb	-10.2	-7.16	-8.22	-16.3
Dy	-9.89	-6.79	-8.29	-16.5
Ho	-10.0	-6.85	-8.35	-16.7
Er	-10.0	-6.86	-8.39	-16.7
Tm	-10.1	-6.91	-8.42	-16.8
Yb	-10.1	-6.89	-8.42	-16.9

Table S4. Average distances ($r_{Ln..H}$) and angles with respect of the molecular axis ($\theta_{Na\text{-}Ln\text{-}H}$) for the acetate protons (H(Me)) in the Gd^{III}/Yb^{III}-MC series (see labelling in Figure 3 and here below). Data obtained from the X ray crystal structure.[9] The angles between the nucleus under consideration and the principal magnetic axis of the lanthanide ion has been approximated into the Na^{I}-Ln^{III} direction. Distances and angles have been averaged over the twelve protons.

	$r_{Ln..H}$ (Å)	$\theta_{Na\text{-}Ln\text{-}H}$ (°)
Gd	4.968	57.06
Tb	4.945	56.83
Dy	4.936	56.60
Ho	4.926	56.19
Er	4.914	55.86
Tm	4.896	55.61
Yb	4.891	55.52

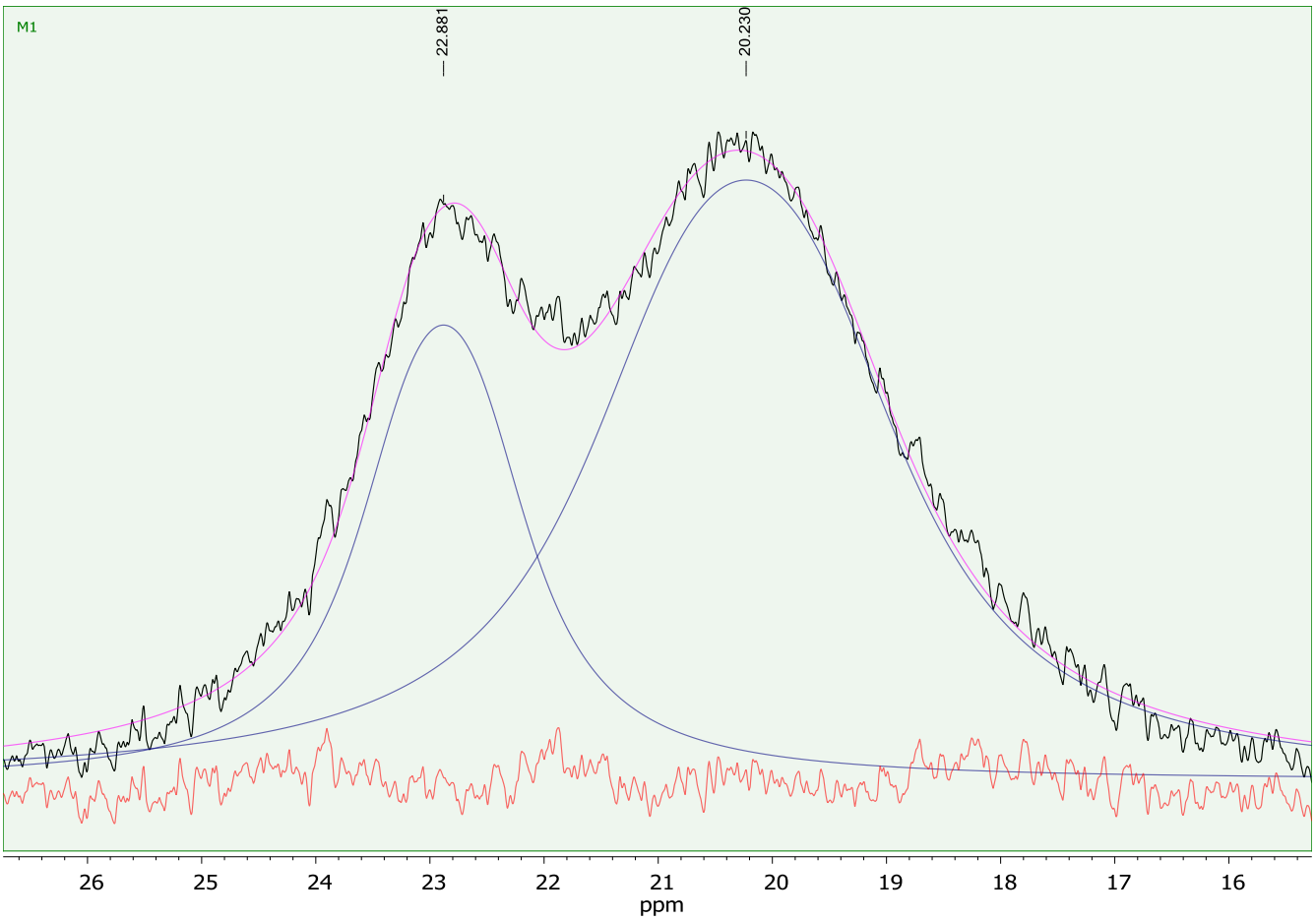

Figure S1. Deconvolution of the overlapped 1 and Me signals (23 and 20 ppm, respectively) in the spectrum of Dy^{III}-MC. Black: observed spectrum; blue: deconvolution functions; purple: calculated spectrum; red: residual function (observed – calculated). The relative integral of the two functions corresponds to 1:3 ratio.

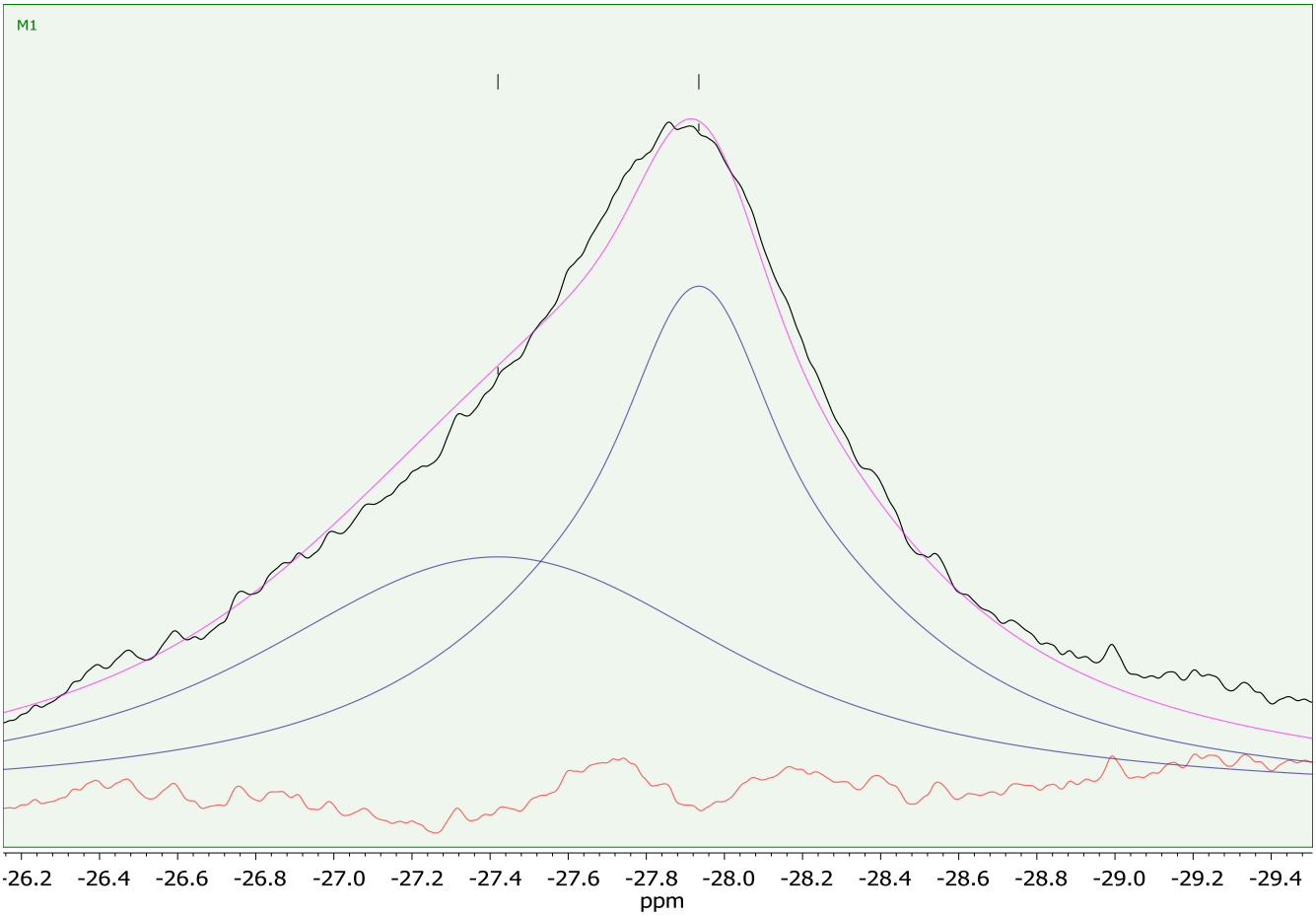

Figure S2. Deconvolution of the overlapped 2 and 3 signals (-27.4 and -28.0 ppm, respectively) in the spectrum of Tm^{III}-MC. Black: observed spectrum; blue: deconvolution functions; purple: calculated spectrum; red: residual function (observed – calculated). The relative integral of the two functions corresponds to 1:1 ratio.

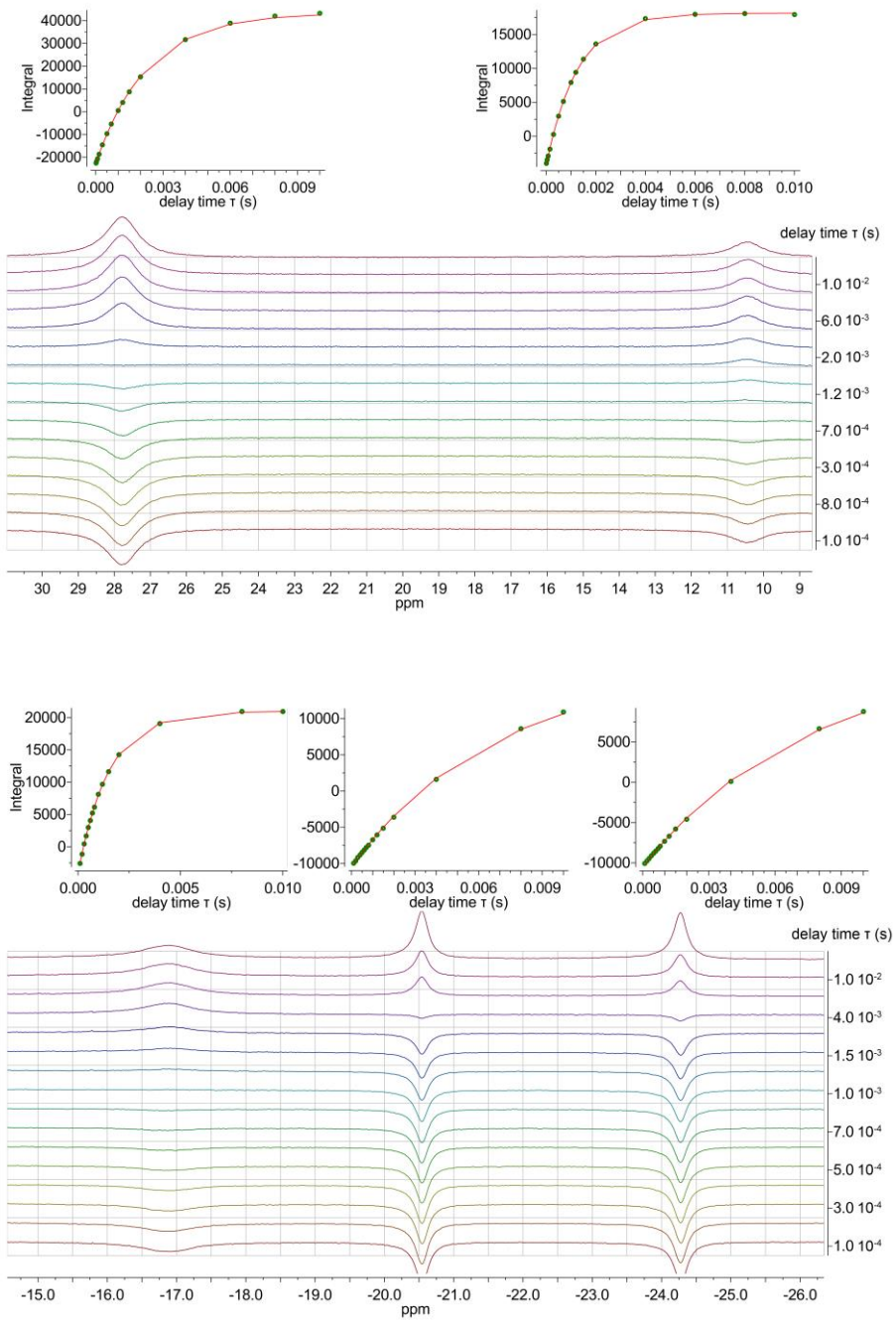

Figure S3. Representative inversion recovery data and fitting for the $Y^{III}Na^{I}(OAc)_4$[12-$MC_{Mn^{III}(N)}$shi-4]$(H_2O)_4$·6DMF complex in deuterated methanol.

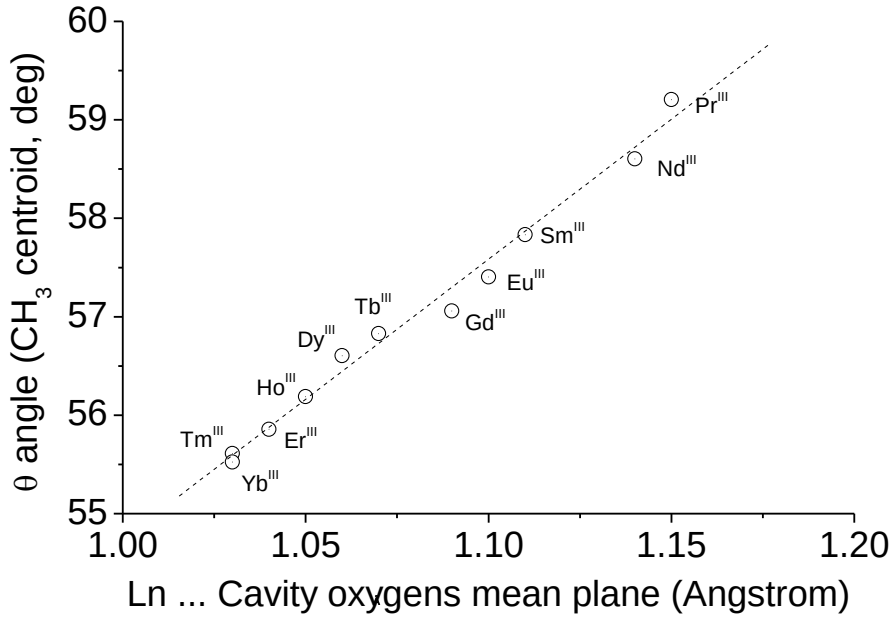

Figure S4. Average theta (*θ*) angles (calculated from X ray structures) of the CH_3 centroids as a function of the distance between the Ln^{III} and the mean plane of the cavity oxygens.

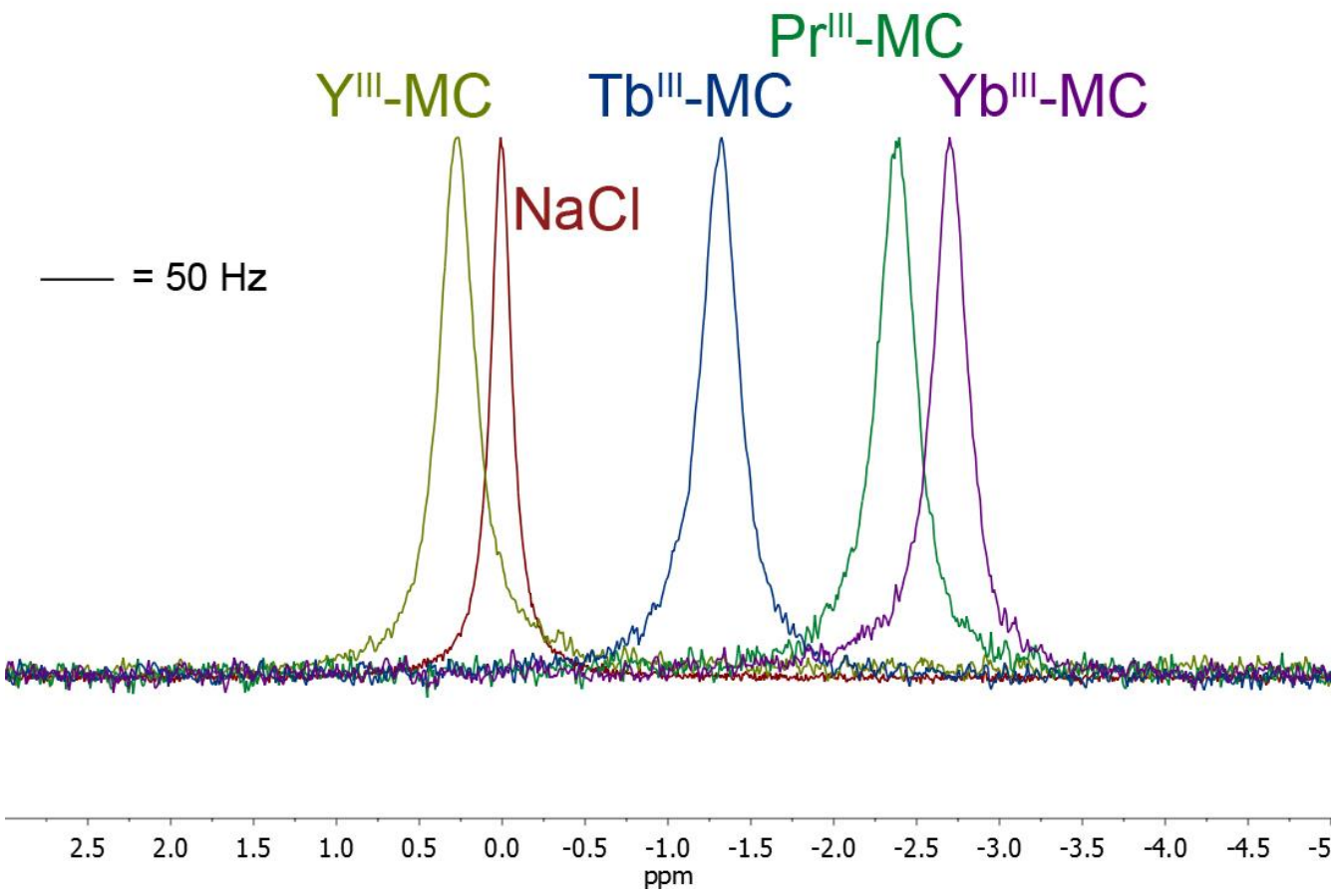

Figure S5. ^{23}Na-NMR spectra of Y^{III}-, Pr^{III}-, Tb^{III}- and Yb^{III}-MC complexes in methanol-d_4, along with that of NaCl.

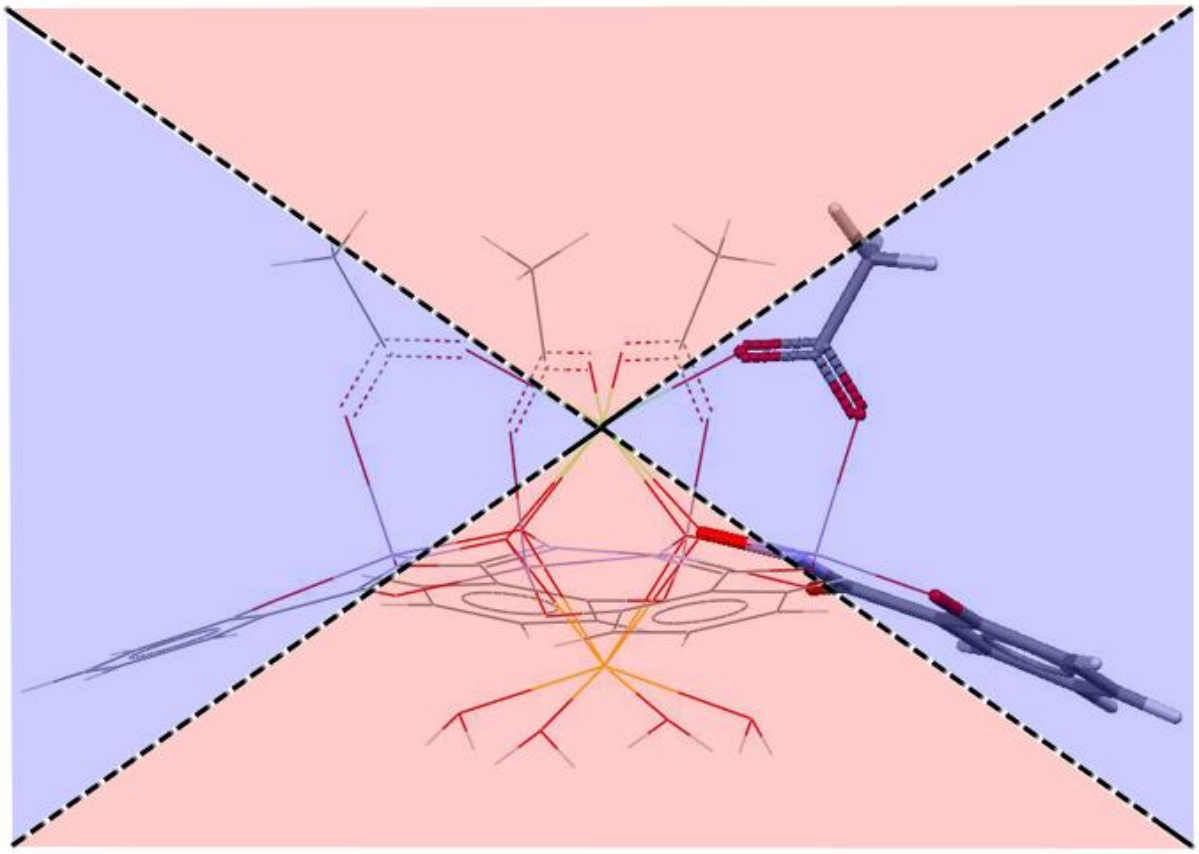

Figure S6. Single crystal X-ray structure of $Y^{III}Na^{I}(OAc)_4[12\text{-}MC_{Mn^{III}(N)shi}\text{-}4](H_2O)_4 \cdot 6DMF$. Light green = Pr^{III}, purple = Mn^{III}, yellow = Na^{I}. Protons in the red conical volume are associated with positive G(i) values, while those in the blue volume with negative G(i) values.

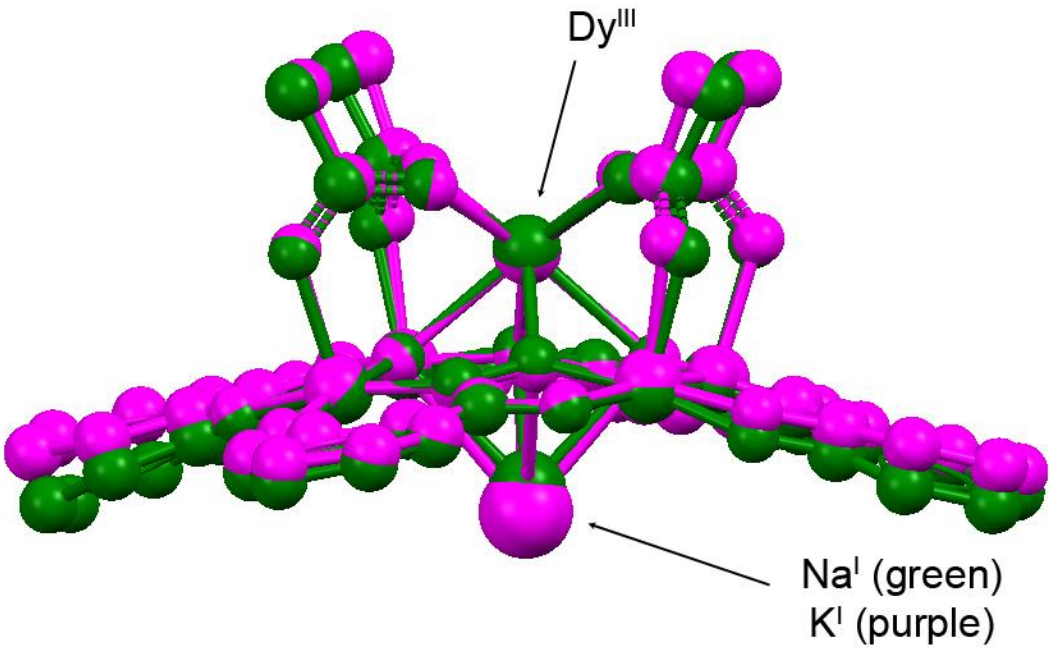

Figure S7. Overlay of the structures of $Dy^{III}Na^{I}(OAc)_4[12\text{-}MC_{Mn^{III}(N)}shi\text{-}4](H_2O)_4\cdot 6DMF$ (Dy^{III}-MC, purple) and $(Dy^{III}K^{I}(OAc)_4[12\text{-}MC_{Mn^{III}(N)shi}\text{-}4](DMF)_4\cdot DMF$ (green). Solvent molecules have been omitted for clarity. The overlayed structures show that upon changing Na^{I} with K^{I} (green into purple) the MC framework results in a less domed structure with the Dy^{III} ion more encapsulated in the cavity and the acetate ligands more aligned with the *z*-axis.

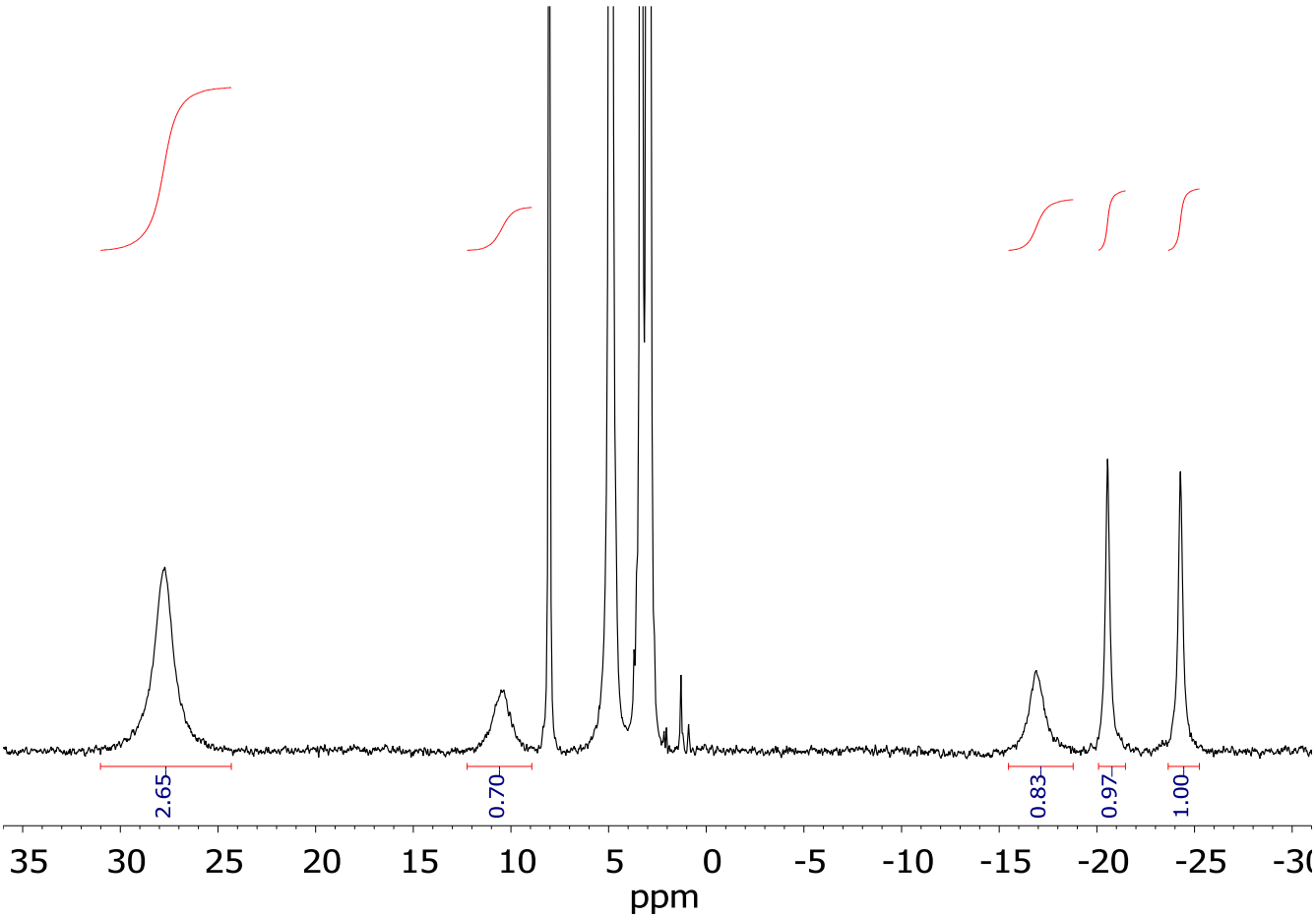

Figure S8. ^{1}H NMR spectrum of $Y^{III}Na^{I}(OAc)_4[12\text{-}MC_{Mn^{III}(N)shi}\text{-}4](H_2O)4\cdot6DMF$ in CD_3OD.

REFERENCES:

(1) Bertini, I.; Luchinat, C. Chapter 5 Magnetic Coupled Systems. In *NMR of Paramagnetic Substances*; Lever, A. B. P., Ed.; Coordination Chemistry Reviews; Elsevier, 1996; pp 131–161.

(2) Bertini, I.; Luchinat, C. Chapter 3 Relaxation. *Coord. Chem. Rev.* **1996**, *150*, 77–110 DOI: 10.1016/0010-8545(96)01243-X.

(3) Eaton, D. R. The Nuclear Magnetic Resonance of Some Paramagnetic Transition Metal Acetylacetonates. *J. Am. Chem. Soc.* **1965**, *87* (14), 3097–3102 DOI: 10.1021/ja01092a015.

(4) La Mar, G. N.; Walker, F. A. Proton Nuclear Magnetic Resonance Line Widths and Spin Relaxation in Paramagnetic Metalloporphyrins of chromium(III), manganese(III), and iron(III). *J. Am. Chem. Soc.* **1973**, *95* (21), 6950–6956 DOI: 10.1021/ja00802a014.

(5) Koenig, S. H.; Brown, R. D.; Spiller, M. The Anomalous Relaxivity of Mn3+(TPPS4). *Magn. Reson. Med.* **1987**, *4* (3), 252–260 DOI: 10.1002/mrm.1910040306.

(6) Luz, Z.; Silver, B. L.; Fiat, D. O−17 Nuclear Magnetic Resonance of Manganese (III) Tris(Acetylacetonate). *J. Chem. Phys.* **1967**, *46* (2), 469–471 DOI: 10.1063/1.1840690.

(7) Bleaney, B. Nuclear Magnetic Resonance Shifts in Solution due to Lanthanide Ions. *J. Magn. Reson.* **1972**, *8* (1), 91–100 DOI: http://dx.doi.org/10.1016/0022-2364(72)90027-3.

(8) Funk, A. M.; Finney, K.-L. N. A.; Harvey, P.; Kenwright, A. M.; Neil, E. R.; Rogers, N. J.; Kanthi Senanayake, P.; Parker, D. Critical Analysis of the Limitations of Bleaney's Theory of Magnetic Anisotropy in Paramagnetic Lanthanide Coordination Complexes. *Chem. Sci.* **2015**, *6* (3), 1655–1662 DOI: 10.1039/C4SC03429E.

(9) Azar, M. R.; Boron, T. T.; Lutter, J. C.; Daly, C. I.; Zegalia, K. A.; Nimthong, R.; Ferrence, G. M.; Zeller, M.; Kampf, J. W.; Pecoraro, V. L.; Zaleski, C. M. Controllable Formation of Heterotrimetallic Coordination Compounds: Systematically Incorporating Lanthanide and Alkali Metal Ions into the Manganese 12-Metallacrown-4 Framework. *Inorg. Chem.* **2014**, *53* (3), 1729–1742 DOI: 10.1021/ic402865p.